*J Neurophysiol* 104: 3261–3275, 2010.
First published June 30, 2010; doi:10.1152/jn.00093.2010.

# Bicuculline-Induced Chorea Manifests in Focal Rather Than Globalized Abnormalities in the Activation of the External and Internal Globus Pallidus

**Maya Bronfeld,[1] Katya Belelovsky,[1] Yaara Erez,[1] Jenia Bugaysen,[2] Alon Korngreen,[1,2] and Izhar Bar-Gad[1,2]**
[1]*The Leslie and Susan Gonda Multidisciplinary Brain Research Center and* [2]*The Mina and Everard Goodman Faculty of Life Sciences, Bar-Ilan University, Ramat-Gan, Israel*

Submitted 20 January 2010; accepted in final form 28 June 2010

**Bronfeld M, Belelovsky K, Erez Y, Bugaysen J, Korngreen A, Bar-Gad I.** Bicuculline-induced chorea manifests in focal rather than globalized abnormalities in the activation of the external and internal globus pallidus. *J Neurophysiol* 104: 3261–3275, 2010. First published June 30, 2010; doi:10.1152/jn.00093.2010. Chorea is a basal-ganglia (BG) related hyperkinetic movement disorder characterized by irregular continuous involuntary movements. Chorea and related hyperbehavioral disorders may be induced in behaving primates by local microinjections of the $GABA_A$ antagonist bicuculline to the globus pallidus externus (GPe). We performed multielectrode extracellular recordings in the GPe and in the globus pallidus internus (GPi) before, during, and after bicuculline microinjections. Bicuculline led to an increase in the firing rate and a change in the firing pattern of GPe neurons. Two types of abnormal neuronal firing patterns were detected in GPe neurons close to the bicuculline microinjection site: continuous high-frequency activity and bistable activity, in which neurons transitioned between high-frequency and complete cessation of firing. Neuronal activity remained uncorrelated within and between the GPe and the GPi, with no evidence for propagation of the focal GPe abnormal activity downstream to the GPi. Despite reduction in the information capacity of bicuculline-affected GPe neurons, the ability to encode behavioral events was maintained. We found similar responses of GPe neurons to bicuculline in vitro in the rat, suggesting a basic cellular mechanism underlying these abnormal firing patterns. These results demonstrate that chorea is associated with focal neuronal changes that are not complemented by global changes in the BG nuclei. This suggests a mechanism of stochastic phasic alteration of BG control leading to the chaotic nature of chorea. Thus rather than imposing a globalized state of cortical excitability, chorea might be associated with changes in internal information processing within the BG.

## INTRODUCTION

Chorea is a hyperkinetic movement disorder characterized by spontaneous involuntary movements that are continuous, irregularly timed, and randomly distributed (Mark 2004; Wild and Tabrizi 2007). Chorea appears as a symptom in multiple basal-ganglia (BG) related movement disorders such as Huntington's disease (HD), L-dopa–induced dyskinesia in Parkinson's disease, and hemiballism (Crossman 1987; Schrag and Quinn 2000; Wild and Tabrizi 2007). The BG constitute a group of interconnected subcortical nuclei that play a major role in control of movement and behavior through their reciprocal connections with the cortex (Alexander et al. 1986). Input to the BG is sent to the striatum and the subthalamic nucleus (STN) and is conveyed to the thalamus and cortex through the output nuclei: the globus pallidus internus (GPi) and the substantia nigra pars reticulata. Within the BG, information is processed through the interplay of two opposing pathways: the direct path from the striatum to the output nuclei and the indirect pathway, which also involves the globus pallidus externus (GPe) and STN (Albin et al. 1989; DeLong 1990).

Chorea seems to be specifically related to dysfunction in the indirect pathway of the BG circuitry. In HD patients the appearance of chorea is temporally correlated with a selective loss of striatal neurons projecting to the indirect pathway (Allen et al. 2009; Deng et al. 2004; Glass et al. 2000) and damage to the STN was found to be directly related to the appearance of hemiballism both in human patients (Martin 1927; Martin and Alcock 1934) and in nonhuman primates (Carpenter et al. 1950; Hamada and DeLong 1992a). Chorea and other behavioral abnormalities may be induced by local disruptions of γ-aminobutyric acid (GABA) transmission in the indirect pathway. Microinjections of $GABA_A$ antagonists into the motor territory of the primate GPe induce chorea (Crossman et al. 1988; Matsumura et al. 1995), whereas similar injections into the limbic and associative GPe territories induce other forms of excessive abnormal behaviors (hyperbehavioral symptoms), such as hyperactivity and stereotypic behaviors (Grabli et al. 2004). GABA plays a major role in information processing in the GPe since roughly 80% of all synapses within this nucleus are GABAergic (Kita 2007). GABAergic inputs to GPe neurons originate from striatal projections and from GPe collaterals and are mostly mediated by $GABA_A$ ionotrophic receptors (Charara et al. 2000, 2005; Kita et al. 2006; Smith et al. 2001).

Some theoretical models of the BG hypothesize that chorea may result from global reduction of BG output, leading to cortical disinhibition manifesting in the expression of excessive unwanted movements (Albin et al. 1989). Alternative models maintain that the excessive movements may result from focal activation of small neuronal populations in the BG output structures (Mink 2003). Previous studies found that chorea induced by $GABA_A$ antagonists was associated with increased activity in the GPe (Matsumura et al. 1995; Mitchell et al. 1989), accompanied by an augmentation of pauses in some neurons (Matsumura et al. 1995). However, in the GPi, which is the main BG motor output nucleus, more complex changes in activity were observed, consisting of both increases and decreases in firing rate (Matsumura et al. 1995).

The aim of this study was to explore the neuronal correlates of chorea induced by microinjections of the $GABA_A$ antagonist bicuculline in the GPe of nonhuman primates. We used multielectrode recordings of GPe and GPi neurons before and during the expression of chorea to identify changes in the activity

Address for reprint requests and other correspondence: I. Bar-Gad, Bar-Ilan University, Gonda Brain Research Center, Ramat-Gan 52900, Israel (E-mail: bargadi@mail.biu.ac.il).

patterns of single neurons and the interactions between them. In vitro intracellular recordings from the rat GP were used to gain further insights into the effects of bicuculline on these neurons.

## METHODS

### *Animals*

Two *Macaca fascicularis* monkeys (monkeys M and I; male; weight: 4–5 kg) were used in this study. Data from two additional *Macaca fascicularis* monkeys (monkeys A and N) were used as controls for neuronal activity in the normal macaque (details in Erez et al. 2009). The monkeys' health was monitored by a veterinarian and their fluid consumption, diet, and weight were monitored daily. All procedures were in accordance with the National Institutes of Health *Guide for the Care and Use of Laboratory Animals* (1996) and Bar-Ilan University guidelines for the Use and Care of Laboratory Animals in Research. The experiments were approved and supervised by the Institutional Animal Care and Use Committee.

### *Surgical and experimental procedures*

The surgical procedures for cranial implantation are described in detail in previous work from our lab (McCairn et al. 2009). Briefly, two square cilux chambers (27 × 27 mm) (Alpha-Omega Engineering, Nazareth, Israel) were implanted stereotaxically to allow bilateral access to the basal ganglia using a coronal approach. The recording chambers were tilted at 40° (monkey M) or 35 ° (monkey I) in the coronal plane, with their center targeted to the center of the GPi: stereotactic coordinates A13, L8, and H3 (Szabo and Cowan 1984).

The animals were trained to sit in a primate chair and perform a simple sensorimotor task consisting of pressing a central button followed by a press of one of two possible side buttons, depending on a visual cue, for delivery of a liquid reward. Spontaneous behaviors and task execution were observed and recorded during experimental sessions using a multichannel video system (GV-800; GeoVision, Taipei, Taiwan) and digital feedback from the behavioral system. The animal's behavior was monitored 20–40 min prior to injection and 40–120 min after injection. Detailed behavioral analyses were performed off-line using the recorded video based on previously described methods used in this model (Grabli et al. 2004) and by automatic detection of events related to performance of the behavioral task.

### *Electrophysiological recording*

Following recovery from surgery each animal underwent microelectrode guided mapping of the GPe and GPi. The preliminary mapping process was followed by the experimental sessions. The recording and injection setup are described in detail in Supplemental Material S1.[1] Briefly, the injectrode was comprised of a 28-gauge stainless steel cannula with a straight tip that was partially encapsulated inside a piercing cannula (25-gauge OD stainless steel cannula with a beveled tip). During each experimental session ≤11 glass-coated tungsten microelectrodes (impedance 250–750 kΩ at 1 kHz) and the injectrode were introduced using two separate manipulating towers that could move each electrode and the injection cannula independently with 2-μm resolution (Double Microdriving Terminal and Electrode Positioning System; Alpha-Omega Engineering). The tip of the injection cannula was aligned to the tip of the recording electrodes mounted on the same manipulating tower and depth of injection was determined by recordings made through these electrodes. Extracellular activity was filtered by a wide band-pass filter (5–8,000 Hz; 4-pole Butterworth filter), amplified ×2,000 (MCP-Plus; Alpha Omega Engineering) and continuously sampled at 40 kHz (AlphaMap; Alpha-Omega Engineering).

### *Microinjections*

The injection cannula was connected via a Delrin manifold to a 10 μl syringe (Hamilton, Reno, NV) and filled with the injected solution. We used bicuculline methiodide (Sigma-Aldrich, Rehovot, Israel), dissolved in physiological saline at a concentration of 15 μg/μl (29.5 mmol/l) or saline for control injections. At the beginning of each recording day electrodes were lowered into the brain and the GPe and GPi were identified. Subsequently, the tip of the injection cannula was positioned at the chosen site within the GPe and was left in place during the entire experimental session. Once a sufficient number of separable neurons had been identified on the electrodes and were stable for a minimum of 3 min, bicuculline (1–3.5 μl) or saline (1.5–2 μl) was injected manually at a rate of about 2 μl/min. Additional microinjections into the sensorimotor striatum were administered using the same apparatus in separate recording days; results were described in detail in a previous work (McCairn et al. 2009).

### *Analysis of neuronal activity*

Action potentials of individual neurons were sorted off-line (Offline-Sorter V2.8.7; Plexon, Dallas, TX), enabling high-fidelity neuronal identification. Neurons were retained for analysis if they met the following criteria: *1*) The recording was from a location within GPe or GPi. *2*) The acquired neurons' action potentials were of a consistent distinct shape that could be fully separated with a high degree of certainty from the spike waveforms of other neurons and background noise. *3*) The neurons' interspike intervals (ISIs) were confirmed to have a minimum refractory period of 1.5 ms (<0.1% of spikes within the period). *4*) Stable neuronal recording was available for ≥35 s. Some neurons were recorded continuously before and after bicuculline microinjection and the subsequent appearance of abnormal behaviors. The firing rates of these neurons were calculated in 2-s bins for the entire recording period.

All measures in the RESULTS section are presented as mean ± SD unless stated otherwise.

SINGLE-UNIT ANALYSES. Following bicuculline injection, firing patterns of the neurons displayed changes on multiple timescales, ranging from a few milliseconds to multiple seconds. Thus analyses were typically performed in multiple timescales to accommodate the different orders of magnitude in the temporal domain. The ISI distribution was calculated for all neurons using 2-, 10-, and 100-ms bin sizes. Autocorrelation functions were calculated to evaluate both short- and long-term regularity, using ±50 ms and ±10 s offsets in 0.1- and 1-ms bins, respectively. The firing patterns of GPe neurons were first evaluated by an expert human observer and, subsequently, several parameters were tested to quantitatively group the neurons according to their firing patterns. The parameters that gave the best clustering results were: *1*) the inverse of the median ISI [1/median(ISI)] and *2*) the mean length of the longest 1% of ISIs. Thresholds defining the different types of firing patterns were set based on the characteristics of data from normal untreated GPe controls.

DISTANCE FROM INJECTION SITE. The Euclidean three-dimensional distance from the injection site was calculated for each recorded neuron, as given by

$$d = \sqrt{(x_{inj} - x)^2 + (y_{inj} - y)^2 + (z_{inj} - z)^2}$$

where $d$ is the distance (in millimeters); $x$ is the anteroposterior coordinate, $y$ is the mediolateral coordinate, $z$ is the ventrodorsal coordinate; and *inj* denotes coordinates of the injection site (defined as the tip of the injection cannula).

[1] The online version of this article contains supplemental data.

INFORMATION CAPACITY. The upper bound of the neurons' ability to transmit information can be defined as the total entropy of the ISI distribution (Stevens and Zador 1996). For each neuron the ISI distribution in 0.5-ms bins was constructed and the entropy was calculated by

$$H_{ISI} = -\sum_{bin=1}^{n} p_{bin} \log(p_{bin})$$

where $p_{bin}$ is the probability of each bin and $n$ is the total number of bins with a nonzero probability.

SPECTRAL ANALYSES. Oscillations were evaluated using the autocorrelation and the power spectral density (PSD) functions of the spike train, downsampled to 1 kHz. The PSD was calculated with Welch's method using multiple scales. High-frequency (HF) oscillations were evaluated by using a 4,096-bin Hanning window that produced about 0.25-Hz spectral resolution. The significance level was set at $P = 0.01$ (normalized to the number of bins), calculated based on the power in the 10- to 500-Hz frequency band. Low-frequency oscillations were evaluated by using a Hanning window of 16,384 bins that produced a spectral resolution of about 0.06 Hz. The significance level was set at $P = 0.01$ (normalized to the number of bins), calculated based on the power in the 0- to 10-Hz frequency band. For each spike train the "main oscillation frequency" was defined as the frequency with the maximal power of all the frequencies that exceeded the threshold, within the frequency band of interest (10–500 or 0–10 Hz for high and low frequencies, respectively). Coherence was used to study the degree of interaction, as function of frequency, between pairs of neurons. The coherence function is the cross-spectrum of the two traces normalized by their autospectra, yielding values between zero (no coherence) and one (maximal phase correlation). The parameters used for coherence calculation were the same as those for the PSD calculations. Coherence was considered significant ($P < 0.01$) if it crossed the value given by: $limit = 1 - (1 - \alpha)^{1/(N-1)}$, where $\alpha = 0.99$ and $N$ is the number of consecutive windows used for coherence calculation (Rosenberg et al. 1989).

CORRELATION ANALYSIS. Spike-to-spike cross-correlations were calculated for pairs of neurons with overlapping periods of stable recording. Only neuronal pairs that were recorded by different electrodes were included to avoid possible artifacts in the cross-correlation functions (Bar-Gad et al. 2001). The cross-correlation functions were calculated for ±4-s offset, using 1-ms bins. Significance tests were performed by calculating the mean correlation values and SD of the first and last 1-s windows of the cross-correlation function. Confidence levels were calculated based on these parameters at a threshold of $P = 0.01$, normalized to the number of bins. A peak or trough was considered significant if it crossed these thresholds and was within ±300 ms offset from zero.

ANALYSIS OF PERIEVENT NEURONAL ACTIVITY. Time stamps of events of interest were used to construct perievent histograms (using 10-ms bins) of the neuronal data. Significance testing of neuronal activity in perievent histograms was determined by constructing 99% confidence limits based on the mean and SD of the activity within the tail of the histogram (i.e., activity at 5 to 1 s prior to the task-related event).

### *Histology*

Following completion of the experiment, animals were anesthetized using ketamine (10 mg/kg) and stereotactic marking microlesions (DC current 60 μA for 30 s) were made. The lesions were targeted to dorsal white matter tracts at the anatomical plane that was derived from electrophysiological mapping to be consistent with the position of the anterior commissure (AC0) (McCairn et al. 2009). The animals were then deeply anesthetized using sodium pentobarbital (50 mg/kg) and transcardially perfused with 1 liter of physiological saline, followed by 1 liter of 4% paraformaldehyde. The whole brain was removed and buffered in graded sucrose solution 10–30% over 7 days. The brain was then frozen at −25°C and cut in the coronal plane using a cryostat (Leica Microsystems). Each section was digitized using a 10 MPixel digital camera and sections of interest were mounted onto glass slides and Nissl stained. Contours of brain structures were traced using the digitized images and the anteroposterior position of each injection site was plotted on coronal planes, taking AC0 as the origin of the system axes.

### *In vitro slice preparation and recording*

Thick sagittal slices (300 μm) were obtained from the somatosensory cortex, the striatum, and the GP of 12- to 21-day-old Wistar rats killed by rapid decapitation in accordance with the guidelines of the Bar-Ilan University animal welfare committee, using previously described techniques (Bar-Yehuda et al. 2008; Stuart et al. 1993). Slices were maintained in artificial cerebrospinal fluid containing (in mM): 125 NaCl, 2.5 KCl, 25 $NaHCO_3$, 1.25 $NaHPO_4$, 2 $CaCl_2$, 1 $MgCl_2$, 25 glucose, and 0.5 Na-Ascorbat (pH 7.4 with 95% $O_2$-5% $CO_2$, 310 mosmol/kg). Bicuculline methiodide (50 μM) was added to the bath solution via the perfusion system. Complete substitution of the bath medium took <5 min. The experiments reported here were carried out at 34°C. The GP nucleus and individual GP neurons were visualized using infrared differential interference contrast microscopy. The standard pipette solution contained (in mM): 130 K-gluconate, 10 KCl, 10 HEPES, 4 MgATP, 10 Na-phosphocreatin, 0.5 EGTA, and 0.3 GTP (Sigma) (pH 7.2 with KOH, 312 mosmol/kg). Whole cell current-clamp recordings were performed from the soma of GP neurons with the Axopatch-200B (Axon Instruments) amplifier. Voltage was filtered at 10 kHz and sampled at 20 kHz using patch pipettes (4–8 MΩ) pulled from thick-walled borosilicate glass capillaries (2.0 mm OD, 0.5 mm wall thickness; Hilgenberg, Malsfeld, Germany). Some excitatory input to the GP may have been severed by the slicing procedure. To offset the reduced excitation a constant current of 20 pA was injected via the patch pipette throughout the experiment.

The rodent GP is functionally and anatomically homologous to the primate and human GPe (Gerfen and Wilson 1996). Therefore for greater clarity the rodent GP will also be referred to as the GPe.

### *Software*

The MATLAB (MATLAB 2007B; The MathWorks, Natick, MA) software used for data analysis in this article can be found at: http://neurint.ls.biu.ac.il/software/Chorea.

## RESULTS

A total of 20 bicuculline microinjections (Table 1) and 6 saline (Table 2) control microinjections were administered, targeting the GPe in two monkeys (10 bicuculline and 3 saline injections in each monkey). Localization of the injection sites was done using microlesion markings and electrophysiological mapping; the sites were overlaid on the postmortem anatomical reconstruction of the brain (detailed in McCairn et al. 2009). The injection sites were all within the GPe, spanning the anteroposterior levels AC0 to AC-5 (Fig. 1).

### *Behavioral effects*

Normal behavioral patterns of the animals were characterized based on observations made prior to microinjection during each recording day. Abnormal behaviors were observed following 17/20 bicuculline microinjections and were categorized into three previously defined hyperbehavioral states (Grabli et al. 2004) based on the observed behaviors: motor dysfunction,

TABLE 1. *Bicuculline microinjections: anatomical and behavioral details*

| Animal | Injection Number | Side | AC Plane | Volume, μl | Behavioral Effect | | | Latency, min |
|---|---|---|---|---|---|---|---|---|
| | | | | | Limbic | Associative | Motor | |
| M ($n$ = 10) | 1 | L | −1.0 | 2.0 | | (++) | | 7 |
| | 2 | L | −2.0 | 3.0 | | (+) | | 4 |
| | 3 | L | −2.0 | 2.0 | | | | NA |
| | 4 | R | −5.0 | 2.0 | | | (+++) | 6 |
| | 5 | R | −1.0 | 2.0 | (+) | | (++) | $1^L$, $10^M$ |
| | 6 | R | −1.0 | 2.0 | (+) | (++) | | $1^L$, $16^A$ |
| | 7 | R | −0.5 | 2.0 | (+++) | (+) | | $5^L$, $40^A$ |
| | 8 | R | 0.0 | 1.0 | (+++) | (+) | | $5^L$, $20^A$ |
| | 9 | R | −4.0 | 2.0* | | | (+) | 10 |
| | 10 | R | −3.0 | 2.0 | (+) | | (+++) | $2^L$, $5^M$ |
| I ($n$ = 10) | 11 | L | −1.0 | 1.5 | | (++) | (++) | $2^M$, $8^A$ |
| | 12 | L | −1.0 | 1.5 | | | (+++) | 4 |
| | 13 | L | −2.0 | 3.5* | | | | NA |
| | 14 | L | −2.0 | 1.7 | | (++) | (+) | $20^M$, $30^A$ |
| | 15 | L | −4.0 | 2.2* | | | (++) | 3 |
| | 16 | L | −2.0 | 1.5 | | | (+) | 1 |
| | 17 | R | −1.0 | 2.2* | | | (+++) | 10 |
| | 18 | R | −1.0 | 1.5 | | | (+++) | 33 |
| | 19 | R | −2.0 | 1.5 | | | (+) | 10 |
| | 20 | R | −3.0 | 2.2* | | | | NA |

* Over several injections during the session. (+) marks the intensity of the behavioral effect, from (+) mild to severe (+++). When several effects were present together, letters indicate corresponding latencies (*L,* limbic; *A,* associative, *M,* motor).

associative dysfunction, and limbic dysfunction (Supplemental Video S1). Behaviors classified as belonging to a primarily motor dysfunction were abnormal choreic movements of the limbs contralateral to the injection site. Choreic movements were irregular and complex, usually characterized by internal and external rotation or flexion and extension movements involving either a single or a few contiguous joints or an entire limb. Chorea involved the contralateral lower limb, the upper limb, or both, without any clear somatotopy. A detailed description of associative and limbic dysfunctions can be found in Supplemental Material S2. Twelve microinjections resulted in chorea, presenting either as the only effect (8/12 injections) or mixed with another effect (4/12 injections). Locations of microinjection eliciting the different types of abnormal behaviors generally followed the previously described (Francois et al. 2004; Grabli et al. 2004; Haber et al. 1993) functional organization of the GPe: microinjections inducing limbic abnormalities were located at the anterior–ventral part of GPe, associative abnormalities were located at anterior–dorsal parts of GPe, and microinjections eliciting chorea were mostly located at posterior parts (Fig. 1). No abnormal behaviors were observed following any of the saline microinjections (Fig. 1, black markers). The first signs of abnormal movements were usually apparent within minutes following bicuculline microinjection (mean latency to first effect 7.3 ± 8.2 min, Table 1). Chorea typically appeared gradually, with initial mild effects increasing in severity over several minutes. The effect would usually wax and wane over time, with the animal displaying alternating periods of severely abnormal and seemingly normal or mildly abnormal behavior. The abnormal movements usually dissipated toward the end of recording sessions, lasting 30–120 min.

TABLE 2. *Saline microinjections*

| Animal | Injection Number | Side | AC Plane | Volume, μl |
|---|---|---|---|---|
| M | S1 | L | −1 | 2.0 |
| | S2 | L | −5 | 2.0 |
| | S3 | L | −5 | 2.0 |
| I | S4 | R | −2 | 1.5 |
| | S5 | R | −1 | 1.5 |
| | S6 | R | −2 | 1.8 |

The abnormal behaviors following bicuculline microinjection hindered the animal's performance of the behavioral task, but did not completely abolish it. Choreic movements affecting only the lower limbs mostly did not interfere with upper limb movements required for task execution. During sessions in which chorea appeared in the upper limb, the animals seemed able to temporarily suppress the choreic movements for completion of successful trials, whereas the abnormal movements were still present during the intertrial intervals. Notably, this was true for periods of mild to medium behavioral effects, whereas during periods of very severe chorea the animals were unwilling or unable to engage in the behavioral task.

All subsequent analyses of neurons recorded after bicuculline microinjections were performed only on neurons recorded during sessions in which the injection led to chorea. The neurons used for analyses were recorded during the time periods after the bicuculline microinjection and the ensuing appearance of choreic movements, prior to the end of choreic symptoms. Some neurons were recorded continuously before and after bicuculline microinjection and were analyzed separately. No significant differences were found for any of the neuronal characteristics between animals; thus we pooled the data from both monkeys.

### *Changes in GPe neuronal activity*

The GPe is known to include two main subpopulations of neurons: neurons displaying HF activity with a varying degree of pauses (HFPs) and neurons with low-frequency bursting (LFB) activity (DeLong 1971; Elias et al. 2007). In this study

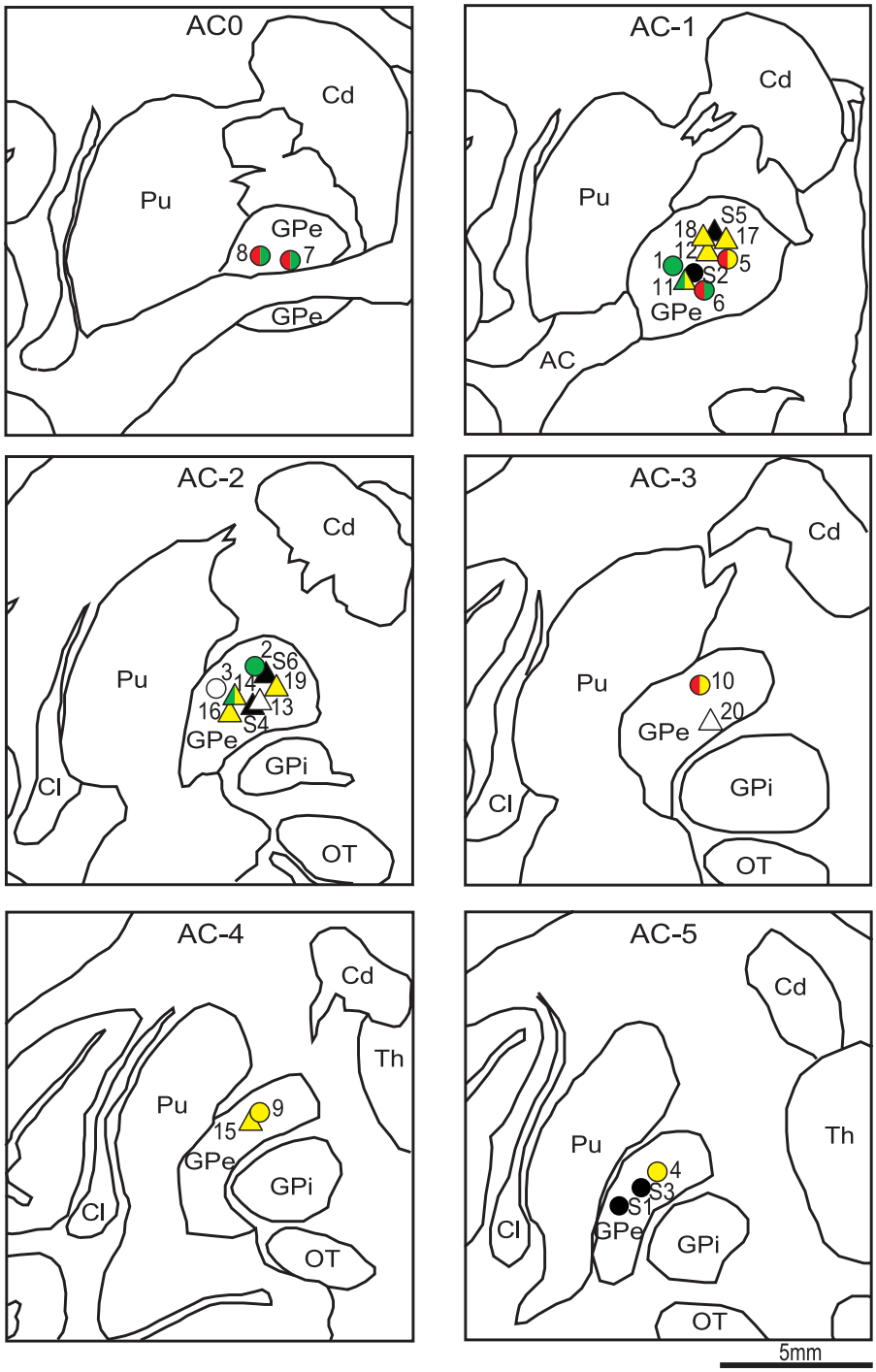


FIG. 1. Anatomical reconstruction of injection site locations. Localization of bicuculline microinjection sites marked according to the evoked abnormal behaviors in monkey M (circles) and monkey I (triangles): chorea (yellow), associative abnormalities (green), limbic abnormalities (red), no effect (white). Injection sites that evoked behavioral abnormalities of more than one type are marked with both colors. The injection sites from both animals are overlaid on the same outlines. Control saline microinjections are marked in black. Outline drawings are reconstructed from the coronal sections (AC0 to AC-5) of the right hemisphere of monkey M. AC, anterior commissure; Cd, caudate nucleus; Cl, claustrum; OT, optic tract; Pu, putamen; Th, thalamus.

we analyzed GPe neurons from each group separately. Seventy-nine stable, well-isolated HF GPe neurons (firing rate >40 spikes/s) recorded after chorea-inducing bicuculline microinjections (monkey I, 65 neurons; monkey M, 14 neurons), 71 HF GPe neurons recorded after saline microinjections (monkey I, 62 neurons; monkey M, 9 neurons), and 80 neurons recorded from the normal untreated GPe (monkey A, 21 neurons; monkey N, 59 neurons) were used for the analyses. The firing rate of neurons recorded after saline microinjection was similar to the firing rate of neurons recorded from the untreated GPe (Fig. 2, *A* and *B*). Bicuculline microinjection caused a marked increase in the overall mean firing rate of GPe neurons (normal 84.6 ± 23.2 spikes/s; saline 83.9 ± 35.5 spikes/s; bicuculline 113 ± 35.9 spikes/s; post hoc Tukey's honestly significant difference [HSD] test, $P < 0.001$; Fig. 2*B*), with many individual neurons maintaining extremely high firing rates (120–230 spikes/s) over extended periods of time (Fig. 2*A*). Seventeen GPe neurons were recorded continuously before and after bicuculline microinjection and the appearance of chorea. Following microinjection 10/17 of these neurons showed significant increase in firing rate (Fig. 2*C*), which was accompanied by changes in firing pattern in 6/10 neurons (Fig. 2*D*).

The firing pattern of most control (untreated and saline-injected) HF GPe neurons followed a Poisson process and had

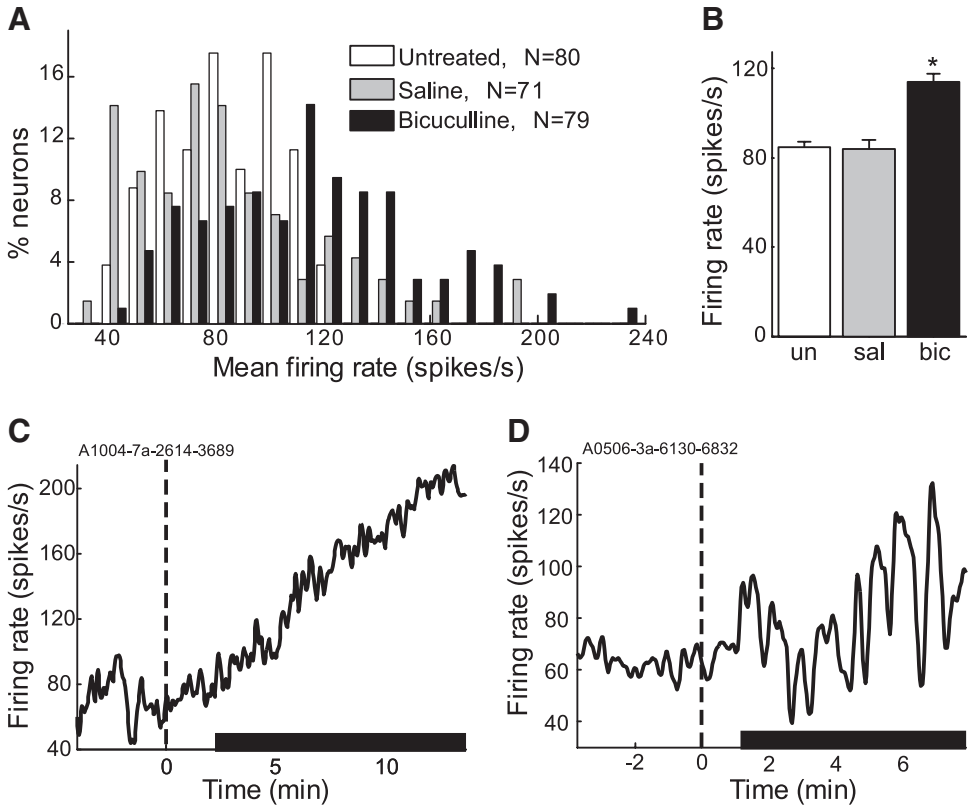


FIG. 2. Neuronal firing rates in the globus pallidus externus (GPe). *A*: distribution of mean firing rates of GPe neurons recorded from an untreated normal macaque (white bars), postsaline microinjection (gray bars), and postbicuculline microinjection (black bars). *B*: comparison of GPe mean firing rates recorded from normal untreated macaque (*un*, white bar), postsaline microinjection (*sal*, gray bar), and postbicuculline microinjection (*bic*, black bar). Error bars indicate SE. *C* and *D*: rate functions, calculated in 2-s bins (smoothed with a Gaussian window with SD = 3.9 s), of GPe neurons recorded continuously before and after bicuculline microinjection and development of chorea. Bicuculline microinjection is marked by the dashed line at *time 0* and the appearance of chorea is marked by the horizontal black line. *C*: a neuron showing a gradual increase in firing rate. *D*: a neuron showing an increase in firing rate and a change in firing pattern. $*P < 0.001$.

a variable degree of pauses (DeLong 1971; Elias et al. 2007). GPe neurons displaying this kind of normal firing pattern were termed high-frequency pausers (HFPs) (Fig. 3*A*). After bicuculline microinjection abnormal firing patterns were observed in many of the recorded neurons. Two types of abnormal patterns were observed and were termed "bistable high-frequency" (BHF) and "continuous high-frequency" (CHF). In BHF neurons, pauses were long and pronounced while the overall firing rate increased, resulting in long trains of very high frequency firing interspersed with periods of complete cessation of spiking activity (Fig. 3*B*). CHF neurons displayed a very high firing rate, firing either continuously or with very few short sparse pauses. Most CHF neurons displayed a regular firing pattern, with narrowly distributed ISIs (Fig. 3*C*). These changes in firing pattern were quantified using two parameters: the inverse of the median ISI (1/median[ISI]) and the mean length of the longest 1% of ISI. The first parameter gives an estimate of the neuron's mean firing rate during the active periods but, unlike the mean, it is not skewed by long pauses. The second parameter identifies neurons with long pauses, thus differentiating between CHF and BHF neurons. Threshold values used for classification of normal and abnormal activity were determined by the distribution of data from the untreated control GPe (Fig. 4*A*, open diamonds). Neurons with an inverse median ISI >145 were classified as having an abnormal firing pattern (bicuculline-affected neurons). Of these affected neurons, neurons with a mean long ISI value of <90 ms were classified as CHF and neurons with larger values were classified as BHF (Fig. 4*A*). This analysis revealed that 44% of GPe neurons recorded after bicuculline injection displayed abnormal activity (20% BHF, 24% CHF), whereas 56% were unaffected (Fig. 4*B*). BHF and CHF neurons were also recorded following control saline injections, but they were less frequent than after bicuculline microinjections ($\chi^2 = 14.4$, degree of freedom [df] = 1, $P < 0.001$): only 20% of the neurons recorded after saline injection were classified as displaying abnormal activity (7% BHF, 13% CHF) (Fig. 4*B*).

Analysis of the distances from injection site revealed a focal spatial distribution of abnormal firing patterns (Fig. 4*C*). The average distance of unaffected neurons from the bicuculline injection site (2.78 ± 1.2 mm, median 3.3) was significantly larger than the distance of neurons classified as BHF (1.49 ± 0.8 mm, median 1.55, post hoc Tukey's HSD test, $P < 0.01$) or CHF (1.77 ± 1.2 mm, median 1.38, post hoc Tukey's HSD test, $P < 0.05$). There was no significant difference between the distances of BHF and CHF neurons. Thus bicuculline-affected neurons were mostly found closer to the injection site compared with unaffected neurons.

The abnormal post-bicuculline firing patterns also affected the ability of GPe neurons to transmit information. The information capacity of BHF and CHF neurons was significantly smaller than that of HFP neurons (post hoc Tukey's HSD test, $P < 0.001$) and the information capacity of CHF neurons was smaller than that of BHF neurons (post hoc Tukey's HSD test, $P < 0.01$) (Fig. 4*D*).

Neurons displaying low-frequency bursting (LFB) activity were recorded in the GPe after bicuculline ($n = 14$) and saline microinjections ($n = 17$). The mean firing rate of these neurons did not differ (saline 23.5 ± 13 spikes/s; bicuculline 21 ± 11.7 spikes/s; *t*-test, $P > 0.1$). However, LFB neurons recorded after bicuculline injection had more pronounced bursting activity, with a smaller incidence of single spikes fired between bursts. There was also a difference in the interburst intervals between

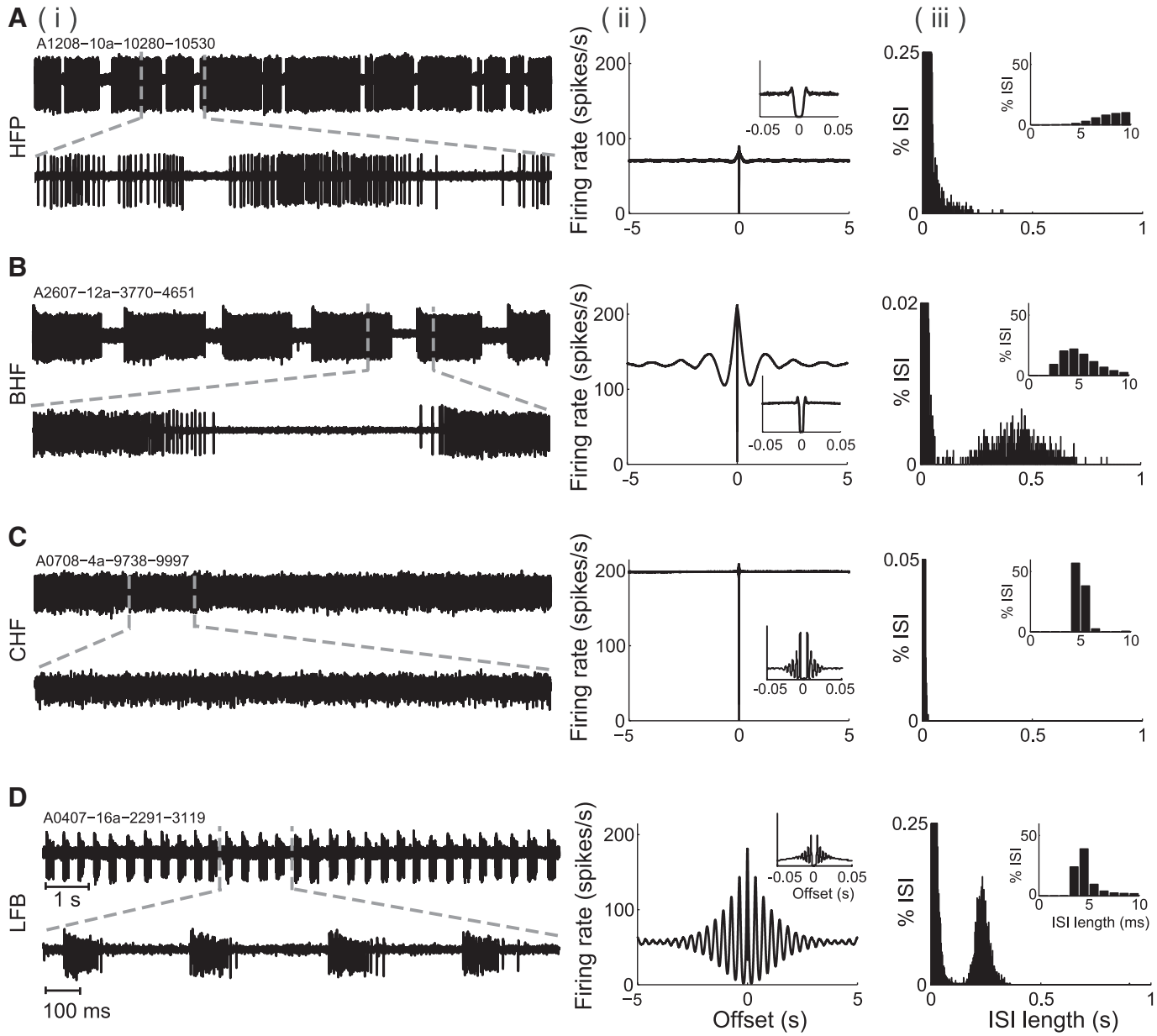


FIG. 3. Postbicuculline GPe firing patterns. Examples of the different types of GPe neurons observed after bicuculline microinjection. *A*: unaffected high-frequency pauser (HFP). *B*: affected bistable high-frequency (BHF) neuron. *C*: affected continuous high-frequency (CHF) neuron. *D*: affected low-frequency burster (LFB). Presented for each neuron are: (*i*) trace of recorded activity at 2 timescales (12 s and inset of 1.5 s), (*ii*) autocorrelation function at 2 timescales (offset ±5 s and inset of ±0.05 s), and (*iii*) interspike interval (ISI) distribution at 2 timescales (0–1 s and inset of 0–10 ms). The *y*-axis of the long-scale ISI histograms is truncated for better examination of long intervals.

the two populations, with bursts of LFB neurons recorded after bicuculline microinjection appearing more regularly (Fig. 3*D*).

### *Oscillations*

HIGH-FREQUENCY OSCILLATIONS. In some bicuculline-affected GPe neurons we observed HF (>100 Hz) oscillatory activity, reflecting the regularity of the spikes (Fig. 5*A*). This regularity was evident in oscillatory peaks in the autocorrelation function calculated with a small offset (<100 ms) (Fig. 3*C*) and peaks in the PSD (Fig. 5*B*). After bicuculline microinjection, regular spiking activity was detected in most CHF (60%, 15/27), but not BHF (4%, 1/24) or HFP (2%, 1/56) neurons. After saline microinjections, regular spiking activity was detected in a small minority of the neurons (1/9 CHF, 0/5 BHF, 6/57 HFP). The mean frequency of the HF oscillations was higher for neurons recorded after bicuculline microinjection compared with neurons recorded after saline microinjection (saline 122.6 ± 45 Hz; bicuculline 195.1 ± 41.3 Hz, *t*-test, $P < 0.001$). Simultaneously recorded neurons displaying regular spiking activity did not oscillate at the same frequency (Fig. 5*B*) and did not show temporally correlated (Fig. 5*C*) or spectrally coherent (Fig. 5*D*) activity.

LOW-FREQUENCY OSCILLATIONS. After bicuculline microinjections very slow oscillations were detected in the activity of some BHF and LFB neurons. This was reflected by oscillatory

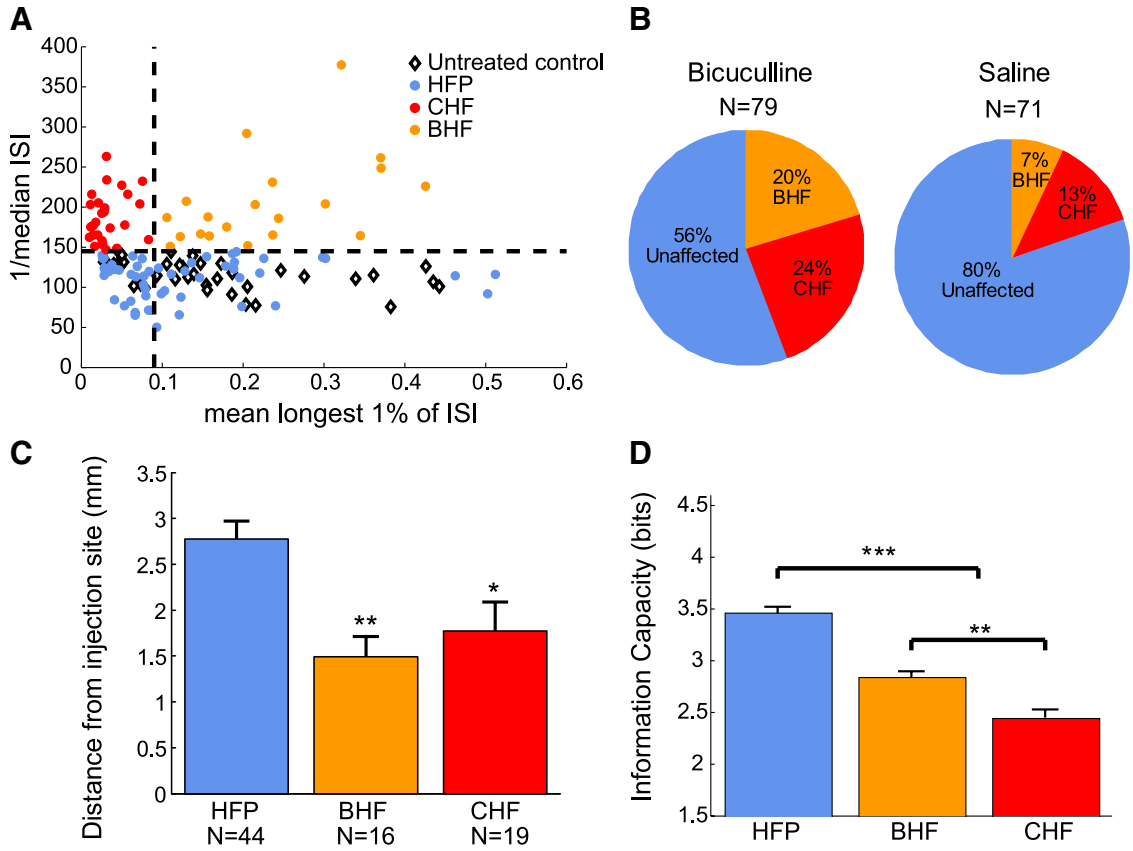


FIG. 4. Properties of the different postbicuculline GPe neuronal groups. *A*: scatterplot of 1/median ISI vs. mean length of longest 1% ISI values for postbicuculline (colored circles) and control untreated GPe neurons (white diamonds). Dashed lines indicate thresholds for the 2 parameters used for the group classification. Blue, unaffected neurons; red, CHF; orange, BHF; color scheme is the same for all the subfigures. *B*: fraction of neurons classified as BHF, CHF, or unaffected recorded after bicuculline and saline microinjections. *C*: mean 3-dimensional (3D) distance from the bicuculline injection site of BHF, CHF, and unaffected GPe neurons. *D*: mean information capacity of BHF, CHF, and unaffected GPe neurons recorded after bicuculline microinjection. Error bars in *C* and *D* indicate SE. $*P < 0.05$, $**P < 0.01$, $***P < 0.001$.

peaks in the autocorrelation functions calculated with an offset of several seconds (Fig. 3, *B* and *D*) and by peaks in the PSD (Fig. 5*B′*). In BHF neurons these slow oscillations reflected the regularity of changes in the bistable state (firing/pausing transitions) and in LFB neurons they reflected the regularity of the bursts. Nine of 24 (37.5%) BHF neurons recorded after bicuculline microinjections and 2/5 (40%) BHF neurons recorded after saline microinjections displayed slow oscillations. The mean oscillation frequency for post-bicuculline BHF neurons was 0.54 ± 0.13 Hz. Ten of 14 (71%) of the LFB neurons recorded after bicuculline microinjections displayed regular bursting, compared with only 1/17 (6%) LFB recorded after saline microinjections. After bicuculline microinjection the mean frequency of the LFB oscillations was 2.2 ± 1.1 Hz. No slow oscillations were detected in other types of GPe neurons, either after bicuculline or saline microinjections. Simultaneously recorded neurons with significantly slow oscillations did not oscillate at the same frequency (Fig. 5*B′*) and did not show temporally correlated (Fig. 5*C′*) or spectrally coherent (Fig. 5*D′*) activity.

### *Changes in GPi neuronal activity*

In all, 64 stable, well-isolated GPi neurons recorded after chorea-inducing bicuculline microinjections (monkey I, 55 neurons; monkey M, 9 neurons), 67 GPi neurons recorded after saline microinjections (monkey I, 59 neurons; monkey M, 8 neurons), and 64 neurons recorded from normal untreated GPi (monkey N, 54 neurons; monkey A, 10 neurons) were used for the following analyses. There were no significant differences in the mean firing rate of GPi neurons recorded under the different conditions (untreated 87.3 ± 19.2 spikes/s; saline 78.3 ± 22.5 spikes/s; bicuculline 82 ± 27.3 spikes/s; one-way ANOVA, $P > 0.05$) (Fig. 6, *A* and *B*). GPi neurons from all conditions displayed the typical continuous random firing pattern (DeLong 1971), with no abnormal firing patterns detected and no oscillatory activity in either the high- or low-frequency ranges.

### *Correlations*

Three types of correlations were examined, based on the location of the simultaneously recorded neurons: GPe–GPe, GPi–GPi, and GPi–GPe correlations (Supplemental Material S3). Very little correlated activity was detected for any of the types of pairs (Fig. 7). There were no significant differences in the fraction of correlated pairs or in the direction of correlation (positive or negative) recorded from normal, saline-injected, or bicuculline-injected GPe and GPi (all $\chi^2$ tests yielded $P > 0.01$). Notably, even significantly correlated pairs showed only weakly correlated activity: <10% maximal change compared with baseline level (Fig. 7).

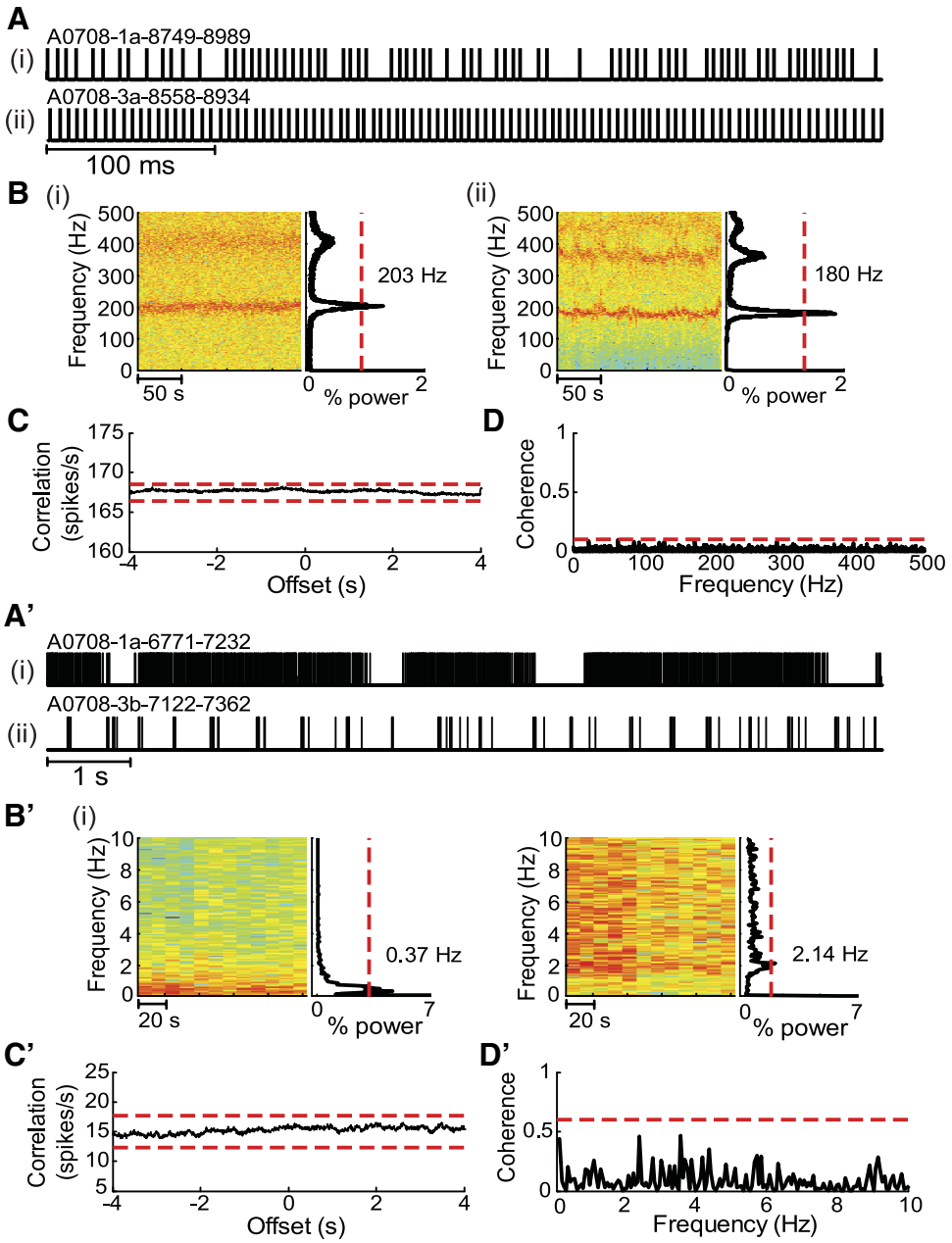


FIG. 5. Postbicuculline neural oscillations in the GPe. Oscillations were observed on 2 scales. *A–D*: high-frequency oscillations (100–500 Hz). *A′–D′*: low-frequency oscillations (0.2–10 Hz). *A*: short traces (500 ms) of 2 simultaneously recorded GPe CHF neurons. Subsequent subfigures (*B–D*) show data for these 2 neurons. *B*: the spectrogram and power spectral density (PSD) of each neuron showing stable high-frequency oscillations. The frequency on the PSD graph is the frequency with maximal power. *C*: the cross-correlation function of the neurons showing zero correlation in the temporal domain. *D*: coherence of the neurons showing no significant coherence in the spectral domain. *A′*: long traces (10 s) of simultaneously recorded BHF (*i*) and LFB (*ii*). Subsequent subfigures (*B′–D′*) show data for these 2 neurons. *B′–D′*: same as *B–D*, respectively, but calculated and presented only for the low-frequency range (0–10 Hz). In all the subfigures, the dashed red lines are the 99% confidence limits.

### *Behavior-related neuronal activity*

TASK-RELATED ACTIVITY. After chorea-inducing bicuculline microinjection 32 HF GPe and 22 GPi neurons were recorded during periods in which the animals performed the behavioral task. Task-related firing rate modulations could be detected in 15/32 HF GPe and 3/22 GPi neurons (Fig. 8). The task-related neuronal responses were diverse, with most neurons responding to movement and some responding to sensory cues or reward. Task-related activity modulations were, in similar proportions, increases or decreases in firing rate. Notably, specific task-related activity modulations could be detected in bicuculline-affected neurons classified as BHF (Fig. 8*A*) or CHF (Fig. 8*B*).

NEURONAL ACTIVITY ASSOCIATED WITH BICUCULLINE-INDUCED ABNORMAL BEHAVIORS. The intermittent nature of chorea observed in this study enabled us to split the data into periods when the animal expressed choreic movements and time periods when the animal was motionless. This analysis did not reveal any rate or pattern changes in the activity of GPe or GPi neurons between time periods of excessive abnormal behavior and periods without movement. During the expression of chorea, attempts to identify repetitive motion segments to which neuronal activity could be aligned were unsuccessful due to the chaotic nature of choreic movements.

### *In vitro effects of bicuculline on rat GPe neurons*

A total of 10 GPe neurons were recorded in vitro from a rat slice preparation. Following bicuculline application all the neurons increased their firing rate and two types of firing patterns were observed (Fig. 9). The first type of neurons (6/10 neurons) displayed a bistable firing pattern, spontaneously shifting between periods of HF firing and periods of hyperpo-

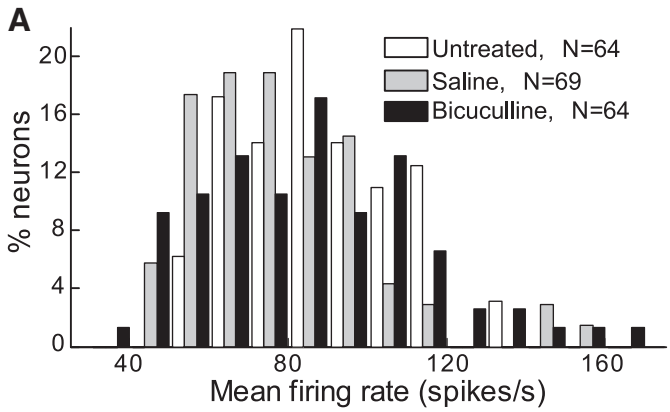


FIG. 6. Post bicuculline neuronal activity in the globus pallidus internus (GPi). *A*: distribution of mean firing rates of GPi neurons recorded from untreated normal macaque (white bars), postsaline microinjections (gray bars), and postbicuculline microinjections (black bars). *B*: comparison of GPi mean firing rates recorded from normal untreated macaque (*un*, white bar), postsaline microinjection (*sal*, gray bar), and postbicuculline microinjection (*bic*, black bar). Error bars indicate SE.

larized membrane potential and no spiking activity (Fig. 9*A′*). Bursts of activity appeared regularly within the bistable process, manifesting as oscillatory peaks in the autocorrelation function and peaks in the low-frequency range of the PSD. The second type of neurons (4/10 neurons) displayed continuous HF firing, occasionally interspersed with short cessations in firing. The spikes were regularly timed, manifesting as oscillatory peaks in the autocorrelation function and peaks in the PSD. During pauses in spiking activity the membrane potential was depolarized and they were preceded by a gradual reduction in the size of the action potentials (Fig. 9*B′*), indicating the pauses were a result of depolarization block.

## DISCUSSION

This work examined the electrophysiological correlates of chorea induced by bicuculline microinjection into the GPe. The behavioral effects in the present study are in line with those

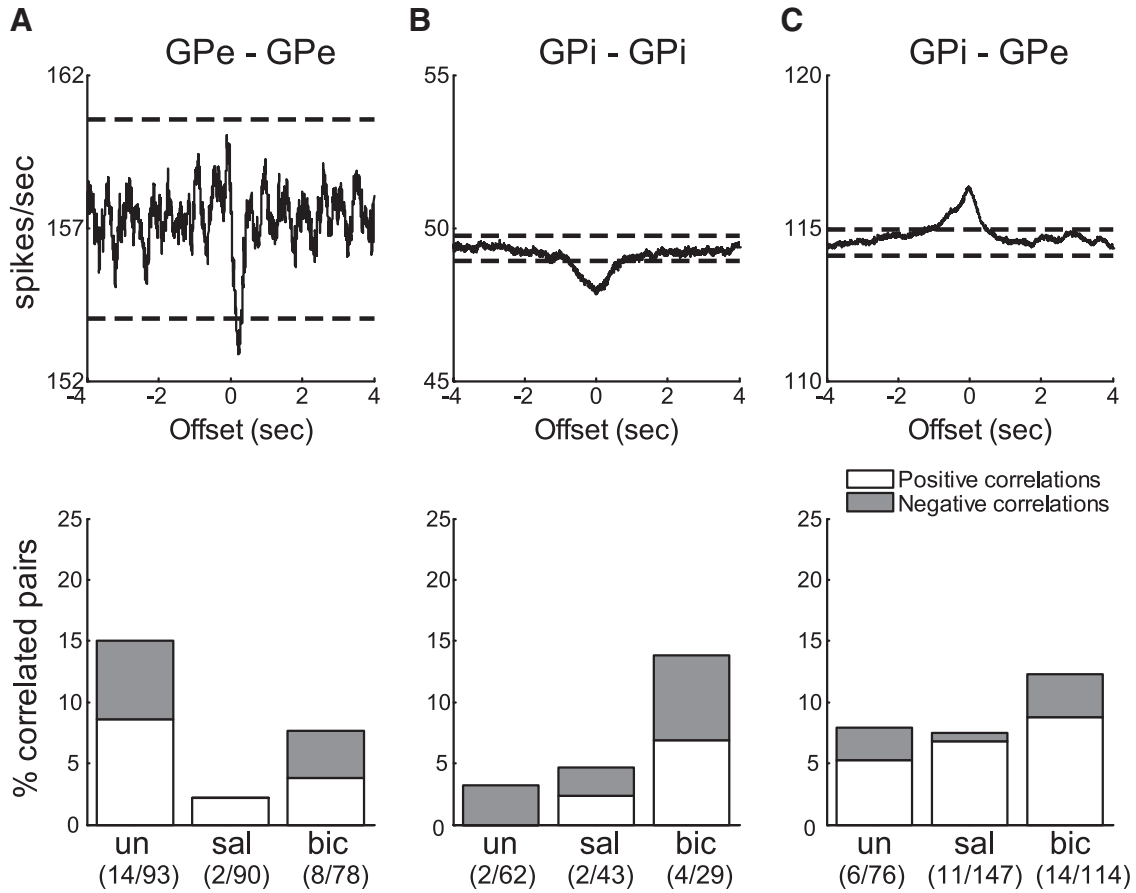


FIG. 7. Cross-correlations in the GPe and GPi following bicuculline microinjection. Cross-correlations are grouped based on the nuclei of the neuronal pairs: GPe–GPe (*A*), GPi–GPi (*B*), and GPi–GPe (*C*). *Top row*: examples of postbicuculline cross-correlation functions calculated in 1-ms bins with ±4-s offset. The *y*-axis represents the conditional firing rate in spikes/s. Dashed lines represent the 99% confidence intervals. The graphs show significant correlations, but the magnitude of the peaks/troughs is very small. *Bottom row*: percentage of correlated pairs in each condition (*un*, untreated normal macaque; *sal*, postsaline microinjections; *bic*, postbicuculline microinjections), divided by the type of correlation (white, positive; gray, negative). The numbers in parentheses presented under each bar are the number of significantly correlated pairs/total number of simultaneously recorded pairs. There were no significant differences in the fraction of correlated pairs between the different conditions (untreated, saline, bicuculline) for any correlation type.

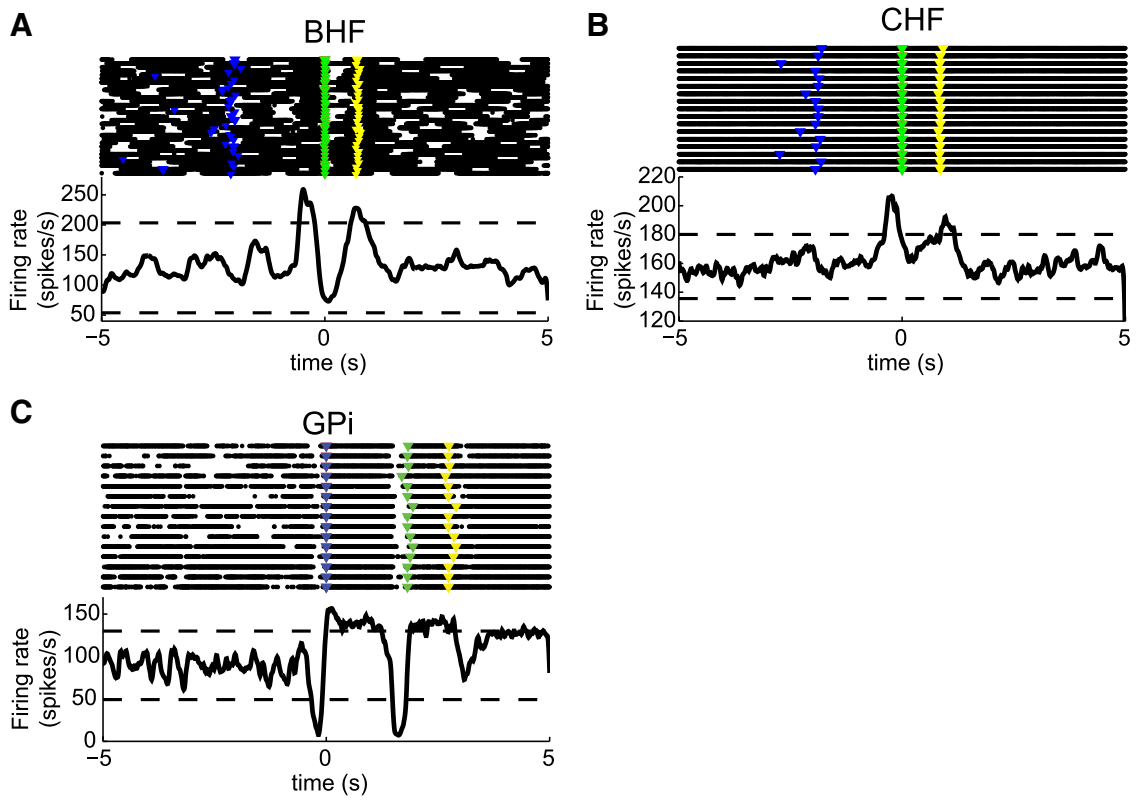


FIG. 8. Postbicuculline movement-related firing rate modulations. *A–C*: behavioral task-related perievent time histograms and raster plots of postbicuculline BHF (*A*), CHF (*B*), and GPi (*C*) neurons. Black dots on the raster represent spikes of the neurons and triangle markers indicate timing of touch central button (blue), touch side button (green), and delivery of liquid reward (yellow). Dashed lines are 99% confidence limits.

described earlier (Grabli et al. 2004), showing a direct relationship between the location of injections in the GPe and the induced abnormal hyperbehavioral symptoms. Bicuculline caused a marked increase in the firing rate of GPe neurons, which was associated with drastic changes in firing pattern. In some bicuculline-affected GPe neurons, pauses became more pronounced (BHF), whereas in others they were almost completely abolished (CHF). These abnormal activity patterns were associated with a reduction in the information capacity of neurons. Bicuculline also induced regularity in both the spiking and bursting activity in the GPe. However, there was very little correlated activity in the GPe either in the temporal or in the spectral domains. There were no gross changes in the activity of GPi neurons after GPe bicuculline microinjection, with overall firing rate, pattern, oscillations, and correlations remaining within normal range. Despite the changes in tonic neuronal activity, bicuculline-affected GPe neurons were still able to encode movements and sensory events.

The two types of abnormally active GPe neurons (BHF and CHF) were detected following bicuculline administration both in vivo (behaving primate) and in vitro (rat slice). In vivo, bicuculline had a focal effect on GPe neurons located within a 1.5- to 2-mm radius around the site of injection, which is in line with estimations of the extent of bicuculline diffusion (Yoshida et al. 1991). Neurons located further away from the injection site were mostly unaffected and displayed normal firing rates and patterns. This suggests that despite the existence of collateral connections between GPe neurons (Kita and Kitai 1994; Sadek et al. 2007), the abnormal firing patterns of the bicuculline-affected neurons did not propagate to other neurons within the nucleus. The localized nature of the bicuculline effect was further evidenced by the spatial organization of the different bicuculline-induced behavioral abnormalities. The nature of abnormal behaviors induced by bicuculline was spatially organized within the nucleus and followed the known anatomical subdivision of the GPe into motor, limbic, and associative territories (Francois et al. 2004; Haber et al. 1993). This suggests that rather than causing a global dysfunction of the GPe, the bicuculline effect is focal in nature and confined to the local area (and functional circuit) surrounding the site of injection.

The changes in firing patterns of GPe neurons brought on by application of bicuculline may be attributed to the block of $GABA_A$ receptors, which alters the patterns of input to the neurons. Because most of the input to GPe neurons is mediated by $GABA_A$ receptors originating either from the striatum (Parent and Hazrati 1995) or from GPe collaterals (Kita and Kitai 1994), bicuculline blocks many of these synapses and thus cuts off the neurons from most of their afferents (Chan et al. 2004). This reduction of inhibitory drive could lead to the observed increase in firing rate of the neurons due to the reduced inhibitory shunt. Thus the two types of firing patterns observed in vitro might result from the unmasking of cellular properties following the block of GABA inputs. One subgroup of neurons responded to bicuculline with a bistable firing pattern (Fig. 9*A′*). One mechanism that could account for this response is the activation of SK channels during the bursts inducing long interburst afterhyperpolarization. SK channels have been shown to influence GP firing patterns (Deister et al. 2009) and to be influenced by bicuculline (Druzin et al. 2004;

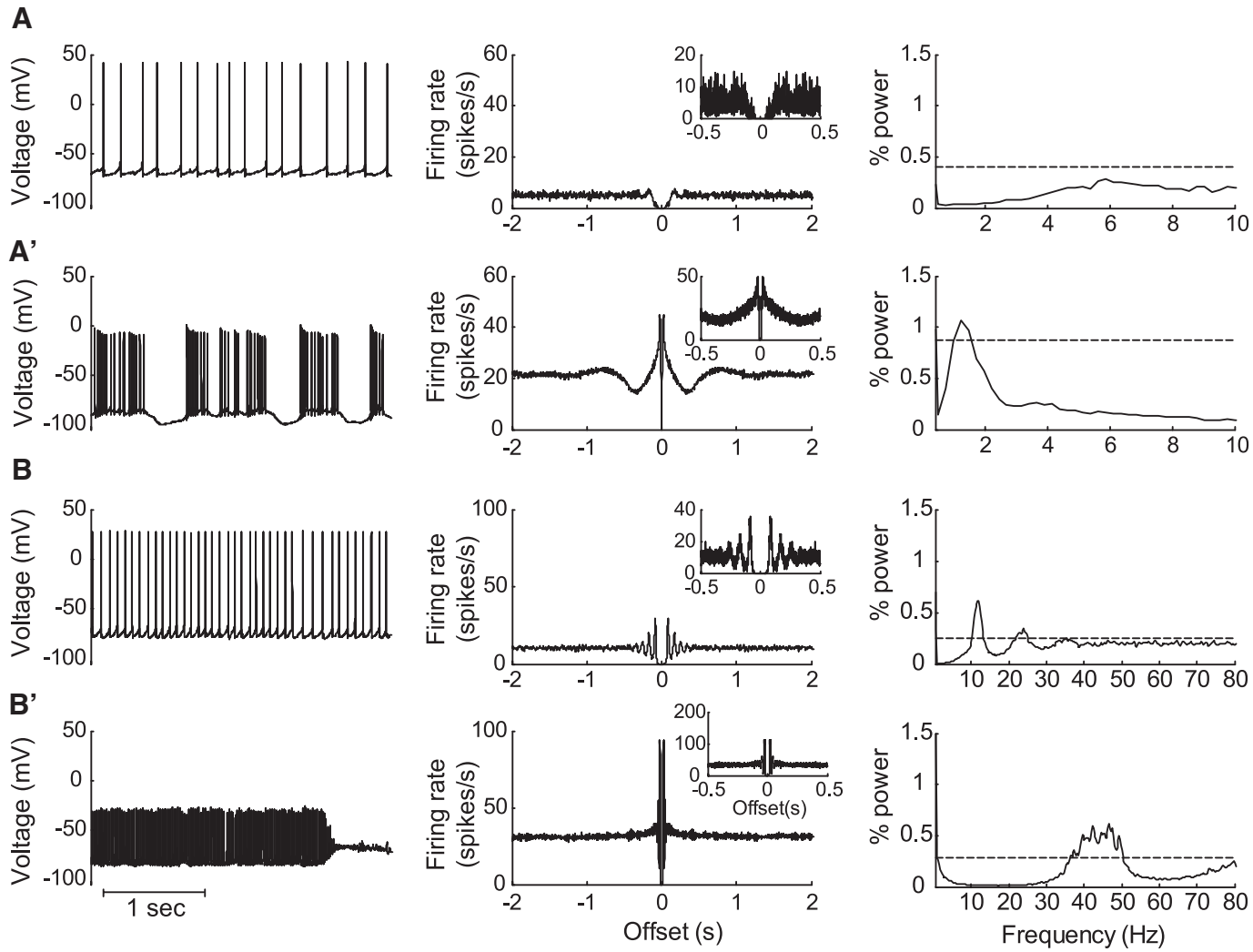


FIG. 9. In vitro effects of bicuculline on rat GPe neurons. Intracellular recording trace, autocorrelation function, and PSD of GPe neurons recorded in vitro (*A* and *B*) before (*A′*) and after (*B′*) bicuculline application. *Left column*: trace of recorded intracellular activity; *middle column*: autocorrelation function at 2 timescales (offset of ±2 s and inset of ±0.5 s); *right column*: PSD; dotted line is 99% confidence limit.

Johnson and Seutin 1997). The other group of neurons responded with an increase in firing frequency and a marked decrease in the action potential amplitude (Fig. 9*B′*). This might be due to a partial depolarization block of the voltage-gated $Na^+$ channels expressed by these neurons. In addition, the same types of abnormal GPe firing patterns, albeit to a significantly smaller extent, were detected following microinjection of saline alone. Saline is not expected to influence GABAergic synapses, but it might have an effect on GPe firing properties via different cellular mechanisms. For example, saline (NaCl) lacks many of the ions normally present in the cerebrospinal fluid; therefore it may change ionic concentrations around the injection site and thus affect the cellular mechanisms modulating neuronal activity. Thus the activation patterns observed in GPe neurons after bicuculline administration may also be affected by cellular mechanisms unrelated to synaptic inputs, again suggesting a localized effect of bicuculline.

Despite the reduction in information capacity and local disruption of GABAergic inputs, some of the bicuculline-affected GPe neurons and downstream GPi neurons still demonstrated firing rate modulations directly associated with the behavioral task, comparable to movement-related responses recorded from pallidal neurons of normal animals (Arkadir et al. 2004; Mushiake and Strick 1995; Turner and Anderson 2005). This suggests that the neuronal connections and activation patterns associated with the performance of a familiar motor task were largely maintained and undisturbed by the focal disruption of $GABA_A$ inputs. In GPe neurons directly affected by bicuculline such phasic responses might be mediated by glutamatergic inputs from the STN (Hanson et al. 2004; Nambu et al. 2000; Wichmann et al. 1994) or GABAergic inputs activating $GABA_B$ receptors (Charara et al. 2000; Galvan et al. 2005; Kita et al. 2006).

The GPi is a major target for GPe projection neurons (Hazrati et al. 1990; Shink and Smith 1995); therefore it is surprising that the significant changes in GPe activation after bicuculline microinjection were not reflected in the activity of GPi neurons. A possible explanation for this may lie in the uncorrelated nature of abnormal GPe activity observed in this study. GPe activation was shown to be able to effectively influence the activity of GPi neurons (Kita 2007), but due to the diffused pattern of GPe–GPi connectivity a synchronized activation of the GPe (or a subgroup of its neurons) is needed to effectively influence the GPi (Kita 2007). Indeed, in normal

animals there is little or no correlated activity between individual GPe–GPi neurons (Elias et al. 2008; Raz et al. 2000). GPe–GPi correlations have been shown to emerge in some pathological conditions in which the GPe neurons throughout the nucleus fire in a synchronized manner (McCairn et al. 2009; Raz et al. 2000).

The GPi is the main output structure of the BG and it is associated primarily with motor activity (DeLong et al. 1985; Turner and Anderson 1997). Current theoretical models of the BG predict that hyperkinetic states such as chorea be associated with a global reduction of GPi activity that will disinhibit the cortex and facilitate the activation of excessive action sequences (Albin 1995; Albin et al. 1989). In the current study we did not find evidence of significant changes in the firing rate, pattern, or synchrony of GPi neurons. Findings from previous studies looking at GPi activity during choreic states are inconsistent and scarce. GPi recordings from Huntington's disease patients have so far yielded mixed results, with some indicating reduced GPi firing rates (Starr et al. 2008) and some showing no change in GPi rate compared with that in Parkinson's disease patients (Tang et al. 2005). Notably, theses studies did not find any modulation in GPi activity that could distinguish choreic and nonchoreic periods (Starr et al. 2008). STN lesions induce both chorea (hemiballism) and a reduced GPi firing rate, but no evidence links the GPi rate modulation to the onset or maintenance of chorea (Hamada and DeLong 1992b; Nambu et al. 2000). A previous study that examined GPi activity associated with chorea induced by GPe bicuculline microinjections found both increases and decreases in GPi activity associated with chorea, such that there was no overall change in GPi firing rate in any one direction (Matsumura et al. 1995).

If chorea is not associated with global changes in the BG output (such as reduced firing rate or increased synchronization) it might be related to dysfunctions of the flow of information through the BG. A focal GABA dysfunction in the GPe, as was used in this study, might interrupt normal information processing within the GPe (Sadek et al. 2007) or disrupt the balance of information going through the direct and indirect pathways (Mink 2003). This type of effect might disrupt the timing of GPi neuronal activation, thus making its signal irrelevant or inappropriate, without causing major changes to the overall level or pattern of GPi activation. Such formation of rogue patterns of GPi activation could lead to unintended releases of cortical motor patterns that are expressed as chorea. The difficulty in identifying such subtle changes in neuronal activity patterns might be related to the nature of chorea itself. In contrast to the repetitive and rhythmic nature of the abnormal movements seen in motor tics (McCairn et al. 2009) or parkinsonian tremor (Findley et al. 1981; Heimer et al. 2006), the abnormal involuntary movements of chorea are characterized by a disorganized, unpredictable, and random presentation (Mink et al. 2007), which maintains a chaotic nature. This presentation confounds attempts to uncover the neuronal encoding of such movements. The modulations in activity of individual GPi neurons or subgroups may encode different segments of the complete behavior but, since these segments are unknown and rarely repeat themselves due to the chaotic manifestation of the complete behavior, they are impossible to detect. Thus individual GPi neurons might still display firing rate modulation in response to specific parts of the abnormal movements, but if these movement-related changes are short and nonrepetitive they may be lost in the overall spontaneous neuronal activity. When looking at the downstream effect of GPi activation on the cortex, rather than imposing a general state of cortical excitability, specific motor patterns may be encoded in the activity of specific GPi neurons and chorea might represent the random activation of these patterns.

Our results suggest that chorea, unlike other disorders of the cortico-BG loop, does not involve global changes in the activation of the GPe itself or its downstream target. Despite the fact that the GABAergic dysfunction was limited to a localized area within the GPe and generated asynchronous activity, it still led to major hyperkinetic symptoms in the animals. Thus it appears that current rate-based models of the cortico-BG circuitry do not reflect the pathophysiology associated with chorea and new models should take into account phasic patterns of activation and the possible effects of internal computation processes within the BG system. Attempts to understand the complex relationship between chorea and neuronal activity might be hindered by the chaotic nature of chorea itself and may require novel and detailed techniques of both behavioral pattern quantification and neuronal data analyses.

## ACKNOWLEDGMENTS

We thank Dr. N. Nagorsky for technical assistance, Dr. K. W. McCairn for help with equipment and recordings, Dr. M. Dror and P. Malmud for help with the animals, and D. Nesselroth for help with the graphics.

## GRANTS

This study was partially supported by Israel Science Foundation Grant 327/09 and a Tourette Syndrome Association grant.

## DISCLOSURES

No conflicts of interest, financial or otherwise, are declared by the authors.

## REFERENCES

**Albin RL.** The pathophysiology of chorea/ballism and parkinsonism. *Parkinsonism Relat Disord* 1: 3–11, 1995.

**Albin RL, Young AB, Penney JB.** The functional anatomy of basal ganglia disorders. *Trends Neurosci* 12: 366–375, 1989.

**Alexander GE, DeLong MR, Strick PL.** Parallel organization of functionally segregated circuits linking basal ganglia and cortex. *Annu Rev Neurosci* 9: 357–381, 1986.

**Allen KL, Waldvogel HJ, Glass M, Faull RL.** Cannabinoid (CB(1)), GABA(A) and GABA(B) receptor subunit changes in the globus pallidus in Huntington's disease. *J Chem Neuroanat* 37: 266–281, 2009.

**Arkadir D, Morris G, Vaadia E, Bergman H.** Independent coding of movement direction and reward prediction by single pallidal neurons. *J Neurosci* 24: 10047–10056, 2004.

**Bar-Gad I, Ritov Y, Vaadia E, Bergman H.** Failure in identification of overlapping spikes from multiple neuron activity causes artificial correlations. *J Neurosci Methods* 107: 1–13, 2001.

**Bar-Yehuda D, Ben-Porat H, Korngreen A.** Dendritic excitability during increased synaptic activity in rat neocortical L5 pyramidal neurons. *Eur J Neurosci* 28: 2183–2194, 2008.

**Carpenter MB, Whittier JR, Mettler FA.** Analysis of choreoid hyperkinesia in the Rhesus monkey; surgical and pharmacological analysis of hyperkinesia resulting from lesions in the subthalamic nucleus of Luys. *J Comp Neurol* 92: 293–331, 1950.

**Chan CS, Shigemoto R, Mercer JN, Surmeier DJ.** HCN2 and HCN1 channels govern the regularity of autonomous pacemaking and synaptic resetting in globus pallidus neurons. *J Neurosci* 24: 9921–9932, 2004.

**Charara A, Heilman TC, Levey AI, Smith Y.** Pre- and postsynaptic localization of GABA(B) receptors in the basal ganglia in monkeys. *Neuroscience* 95: 127–140, 2000.

**Charara A, Paré JF, Levey AI, Smith Y.** Synaptic and extrasynaptic GABA-A and GABA-B receptors in the globus pallidus: an electron microscopic immunogold analysis in monkeys. *Neuroscience* 131: 917–933, 2005.

**Crossman AR.** Primate models of dyskinesia: the experimental approach to the study of basal ganglia-related involuntary movement disorders. *Neuroscience* 21: 1–40, 1987.

**Crossman AR, Mitchell IJ, Sambrook MA, Jackson A.** Chorea and myoclonus in the monkey induced by gamma-aminobutyric acid antagonism in the lentiform complex. The site of drug action and a hypothesis for the neural mechanisms of chorea. *Brain* 111: 1211–1233, 1988.

**Deister CA, Chan CS, Surmeier DJ, Wilson CJ.** Calcium-activated SK channels influence voltage-gated ion channels to determine the precision of firing in globus pallidus neurons. *J Neurosci* 29: 8452–8461, 2009.

**DeLong MR.** Activity of pallidal neurons during movement. *J Neurophysiol* 34: 414–427, 1971.

**DeLong MR.** Primate models of movement disorders of basal ganglia origin. *Trends Neurosci* 13: 281–285, 1990.

**DeLong MR, Crutcher MD, Georgopoulos AP.** Primate globus pallidus and subthalamic nucleus: functional organization. *J Neurophysiol* 53: 530–543, 1985.

**Deng YP, Albin RL, Penney JB, Young AB, Anderson KD, Reiner A.** Differential loss of striatal projection systems in Huntington's disease: a quantitative immunohistochemical study. *J Chem Neuroanat* 27: 143–164, 2004.

**Druzin M, Haage D, Johansson S.** Bicuculline free base blocks voltage-activated $K^+$ currents in rat medial preoptic neurons. *Neuropharmacology* 46: 285–295, 2004.

**Elias S, Joshua M, Goldberg JA, Heimer G, Arkadir D, Morris G, Bergman H.** Statistical properties of pauses of the high-frequency discharge neurons in the external segment of the globus pallidus. *J Neurosci* 27: 2525–2538, 2007.

**Elias S, Ritov Y, Bergman H.** Balance of increases and decreases in firing rate of the spontaneous activity of basal ganglia high-frequency discharge neurons. *J Neurophysiol* 100: 3086–3104, 2008.

**Erez Y, Czitron H, McCairn K, Belelovsky K, Bar-Gad I.** Short-term depression of synaptic transmission during stimulation in the globus pallidus of 1-methyl-4-phenyl-1,2,3,6-tetrahydropyridine-treated primates. *J Neurosci* 29: 7797–7802, 2009.

**Findley LJ, Gresty MA, Halmagyi GM.** Tremor, the cogwheel phenomenon and clonus in Parkinson's disease. *J Neurol Neurosurg Psychiatry* 44: 534–546, 1981.

**Francois C, Grabli D, McCairn K, Jan C, Karachi C, Hirsch EC, Feger J, Tremblay L.** Behavioural disorders induced by external globus pallidus dysfunction in primates. II. Anatomical study. *Brain* 127: 2055–2070, 2004.

**Galvan A, Villalba RM, West SM, Maidment NT, Ackerson LC, Smith Y, Wichmann T.** GABAergic modulation of the activity of globus pallidus neurons in primates: in vivo analysis of the functions of GABA receptors and GABA transporters. *J Neurophysiol* 94: 990–1000, 2005.

**Gerfen CR, Wilson CJ.** The basal ganglia. In: *Handbook of Chemical Neuroanatomy. Integrated Systems of the CNS: Cerebellum, Basal Ganglia, Olfactory System*, edited by Swanson LW, Björklund A, Hökfelt T. Amsterdam: Elsevier Science, 1996, vol. 12, pt. III, p. 371–468.

**Glass M, Dragunow M, Faull RL.** The pattern of neurodegeneration in Huntington's disease: a comparative study of cannabinoid, dopamine, adenosine and GABA(A) receptor alterations in the human basal ganglia in Huntington's disease. *Neuroscience* 97: 505–519, 2000.

**Grabli D, McCairn K, Hirsch EC, Agid Y, Feger J, Francois C, Tremblay L.** Behavioural disorders induced by external globus pallidus dysfunction in primates: I. Behavioural study. *Brain* 127: 2039–2054, 2004.

**Haber SN, Lynd-Balta E, Mitchell SJ.** The organization of the descending ventral pallidal projections in the monkey. *J Comp Neurol* 329: 111–128, 1993.

**Hamada I, DeLong MR.** Excitotoxic acid lesions of the primate subthalamic nucleus result in transient dyskinesias of the contralateral limbs. *J Neurophysiol* 68: 1850–1858, 1992a.

**Hamada I, DeLong MR.** Excitotoxic acid lesions of the primate subthalamic nucleus result in reduced pallidal neuronal activity during active holding. *J Neurophysiol* 68: 1859–1866, 1992b.

**Hanson JE, Smith Y, Jaeger D.** Sodium channels and dendritic spike initiation at excitatory synapses in globus pallidus neurons. *J Neurosci* 24: 329–340, 2004.

**Hazrati LN, Parent A, Mitchell S, Haber SN.** Evidence for interconnections between the two segments of the globus pallidus in primates: a PHA-L anterograde tracing study. *Brain Res* 533: 171–175, 1990.

**Heimer G, Rivlin-Etzion M, Bar-Gad I, Goldberg JA, Haber SN, Bergman H.** Dopamine replacement therapy does not restore the full spectrum of normal pallidal activity in the 1-methyl-4-phenyl-1,2,3,6-tetra-hydropyridine primate model of Parkinsonism. *J Neurosci* 26: 8101–8114, 2006.

**Johnson SW, Seutin V.** Bicuculline methiodide potentiates NMDA-dependent burst firing in rat dopamine neurons by blocking apamin-sensitive $Ca^{2+}$-activated $K^+$ currents. *Neurosci Lett* 231: 13–16, 1997.

**Kita H.** Globus pallidus external segment. *Prog Brain Res* 160: 111–133, 2007.

**Kita H, Chiken S, Tachibana Y, Nambu A.** Origins of GABA(A) and GABA(B) receptor-mediated responses of globus pallidus induced after stimulation of the putamen in the monkey. *J Neurosci* 26: 6554–6562, 2006.

**Kita H, Kitai ST.** The morphology of globus pallidus projection neurons in the rat: an intracellular staining study. *Brain Res* 636: 308–319, 1994.

**Mark MH.** Other choreic disorders. In: *Movement Disorders: Neurologic Principles and Practice*, edited by Watts RL, Koller WC. New York: McGraw-Hill, 2004, p. 639–655.

**Martin JP.** Hemichorea resulting from a local lesion of the brain (the syndrome of the body of Luys). *Brain* 50: 637–651, 1927.

**Martin JP, Alcock NS.** Hemichorea associated with a lesion of the Corpus Luysii. *Brain* 57: 504–516, 1934.

**Matsumura M, Tremblay L, Richard H, Filion M.** Activity of pallidal neurons in the monkey during dyskinesia induced by injection of bicuculline in the external pallidum. *Neuroscience* 65: 59–70, 1995.

**McCairn KW, Bronfeld M, Belelovsky K, Bar-Gad I.** The neurophysiological correlates of motor tics following focal striatal disinhibition. *Brain* 132: 2125–2138, 2009.

**Mink JW.** The basal ganglia and involuntary movements: impaired inhibition of competing motor patterns. *Arch Neurol* 60: 1365–1368, 2003.

**Mink JW, Semrau J, Levy E, Newhouse N.** Kinematics and EMG in human chorea. In: *Proceedings of the 9th Triennial Meeting of the International Basal Ganglia Society* (IBGS). Chevy Chase, MD: IBGS, Abstract 712, 2007.

**Mitchell IJ, Jackson A, Sambrook MA, Crossman AR.** The role of the subthalamic nucleus in experimental chorea. Evidence from 2-deoxyglucose metabolic mapping and horseradish peroxidase tracing studies. *Brain* 112: 1533–1548, 1989.

**Mushiake H, Strick PL.** Pallidal neuron activity during sequential arm movements. *J Neurophysiol* 74: 2754–2758, 1995.

**Nambu A, Tokuno H, Hamada I, Kita H, Imanishi M, Akazawa T, Ikeuchi Y, Hasegawa N.** Excitatory cortical inputs to pallidal neurons via the subthalamic nucleus in the monkey. *J Neurophysiol* 84: 289–300, 2000.

**Parent A, Hazrati LN.** Functional anatomy of the basal ganglia. II. The place of subthalamic nucleus and external pallidum in basal ganglia circuitry. *Brain Res Brain Res Rev* 20: 128–154, 1995.

**Raz A, Vaadia E, Bergman H.** Firing patterns and correlations of spontaneous discharge of pallidal neurons in the normal and the tremulous 1-methyl-4-phenyl-1,2,3,6-tetrahydropyridine vervet model of parkinsonism. *J Neurosci* 20: 8559–8571, 2000.

**Rosenberg JR, Amjad AM, Breeze P, Brillinger DR, Halliday DM.** The Fourier approach to the identification of functional coupling between neuronal spike trains. *Prog Biophys Mol Biol* 53: 1–31, 1989.

**Sadek AR, Magill PJ, Bolam JP.** A single-cell analysis of intrinsic connectivity in the rat globus pallidus. *J Neurosci* 27: 6352–6362, 2007.

**Schrag A, Quinn N.** Dyskinesias and motor fluctuations in Parkinson's disease. A community-based study. *Brain* 123: 2297–2305, 2000.

**Shink E, Smith Y.** Differential synaptic innervation of neurons in the internal and external segments of the globus pallidus by the GABA- and glutamate-containing terminals in the squirrel monkey. *J Comp Neurol* 358: 119–141, 1995.

**Smith Y, Charara A, Paquet M, Kieval JZ, Paré JF, Hanson JE, Hubert GW, Kuwajima M, Levey AI.** Ionotropic and metabotropic GABA and glutamate receptors in primate basal ganglia. *J Chem Neuroanat* 22: 13–42, 2001.

**Starr PA, Kang GA, Heath S, Shimamoto S, Turner RS.** Pallidal neuronal discharge in Huntington's disease: support for selective loss of striatal cells originating the indirect pathway. *Exp Neurol* 211: 227–233, 2008.

**Stevens CF, Zador A.** Information through a spiking neuron. In: *Advances in Neural Information Processing Systems 8*, edited by Touretzky DS, Mozer M, Hasselmo ME. Cambridge, MA: MIT Press, 1996, p. 75–81.

**Stuart GJ, Dodt HU, Sakmann B.** Patch-clamp recordings from the soma and dendrites of neurons in brain slices using infrared video microscopy. *Pflügers Arch* 423: 511–518, 1993.

**Szabo J, Cowan WM.** A stereotaxic atlas of the brain of the cynomolgus monkey (*Macaca fascicularis*). *J Comp Neurol* 222: 265–300, 1984.

**Tang JK, Moro E, Lozano AM, Lang AE, Hutchison WD, Mahant N, Dostrovsky JO.** Firing rates of pallidal neurons are similar in Huntington's and Parkinson's disease patients. *Exp Brain Res* 166: 230–236, 2005.

**Turner RS, Anderson ME.** Pallidal discharge related to the kinematics of reaching movements in two dimensions. *J Neurophysiol* 77: 1051–1074, 1997.

**Turner RS, Anderson ME.** Context-dependent modulation of movement-related discharge in the primate globus pallidus. *J Neurosci* 25: 2965–2976, 2005.

**Wichmann T, Bergman H, DeLong MR.** The primate subthalamic nucleus. I. Functional properties in intact animals. *J Neurophysiol* 72: 494–506, 1994.

**Wild EJ, Tabrizi SJ.** The differential diagnosis of chorea. *Pract Neurol* 7: 360–373, 2007.

**Yoshida M, Nagatsuka Y, Muramatsu S, Niijima K.** Differential roles of the caudate nucleus and putamen in motor behavior of the cat as investigated by local injection of GABA antagonists. *Neurosci Res* 10: 34–51, 1991.